Progress In Electromagnetics Research, Vol. 122, 269–292, 2012

A CIRCULAR SYNTHETIC APERTURE RADAR FOR ON-THE-GROUND OBJECT DETECTION

M. Mohammadpoor[1], R. S. A. Raja Abdullah[1, *], A. Ismail[1], and A. F Abas[2]

[1]Wireless and Photonic Networks Research Centre, Faculty of Engineering, Universiti Putra Malaysia (UPM), 43400 Selangor, Malaysia

[2]Department of Computer and Communication Systems Engineering, Faculty of Engineering, Universiti Putra Malaysia, Serdang, 43400 Selangor, Malaysia

Abstract—Detecting an on-the-ground object is a subject of interest for use in some applications. Foreign Object Detection (FOD), which is an important issue in aviation safety, is a possible application. In this way, radar imaging, has several inherent advantages over other on-the-ground object detection techniques. This paper will introduce a ground-based Circular Synthetic Aperture Radar, which detects and localizes various objects, based on their reflection properties of microwaves. Here, wideband Linear Frequency Modulated (LFM) chirp pulses are employed for the transmission and reception of reflection pulses, both to and from the object under test. Once the pulses are received by the radar, a processing algorithm (proposed later in this paper) is executed to confirm detection. In order to verify the validity of the model, a prototype was developed and a series of field experiments was carried out. The results show that the proposed system has the ability to detect and localize on-the-ground objects with dimensions as small as 2 cm high and 1 cm diameter, located several metres away. Furthermore, the resolution of the system was analysed and results indicate that the system is capable of distinguishing multiple objects in close proximity to each other, which therefore, makes it suitable for FOD applications by some small modifications.

Received 22 August 2011, Accepted 2 November 2011, Scheduled 19 November 2011

* Corresponding author: Raja Syamsul Azmir Raja Abdullah (rsa@eng.upm.edu.my).

1. INTRODUCTION

The primary function of radar technology is to detect and localize objects in free space. However, this technology has numerous application prospects for object detection on the ground. One such application is Foreign Object Detection (FOD) for airport runway scanning. The need for an efficient FOD system is a major concern for the aviation industry, because the presence of small objects can jeopardize the safety of an aircraft as evidenced by the Concorde incident in July 2000. In addition, direct losses due to poor FOD systems are estimated at around 3 to 4 billion US dollars per year globally [1]. The typical threatening foreign object size is approximately 2.5 by 2.5 cm, of which 60% are metals including nuts and bolts [2]. A radar system is preferable for this application, due to its larger coverage area, robustness in poor weather conditions, as well as, its ability to operate unabated for twenty-four hours [3].

In this paper a ground-based Circular Synthetic Aperture Radar (Circular-SAR), used to detect on-the-ground objects, is introduced. Although there is no standard definition for Circular-SAR [4], in most Circular-SAR systems, an airborne radar rotates around the area under surveillance, in such a way, that the scanning area is circumscribed by the sensor trajectory. This increases the aspect angle interval, and hence, allows data collection from different angles [5–7]. Although this model is theoretically optimal, it suffers from many practical limitations for use in ground-based applications. These limitations are solved by the model presented in [8], where the radar sensors exhibit a semi-circular trajectory whose circumference is adjacent to the scanning area, with continuous wave stepped frequency signals to detect objects with a high Radar Cross Section (RCS) at distances below 4 meters in a clutter-free environment. However, the problem associated with this model, is that it can only detect high RCS objects in close proximity. Moreover, the fact that these experiments were conducted in a clutter-free environment makes for an uncertain practical applicability. Commercially, some established FOD systems on the market such as Tarsier® [3], have been mentioned to be effective in object detection at relatively far distances. However, these systems normally use special narrow beam antennas, which emit very high frequency millimetre waves that are prone to affected by harsh environmental conditions, such as rain, fog, and snow. In addition, high frequencies have some difficulties for applications that require wave penetration.

To solve the above-mentioned limitations, this paper proposes a ground-based Circular Synthetic Aperture Radar, capable of detecting

and localizing various objects based on their reflection properties of microwaves. To achieve this, wideband Linear Frequency Modulated (LFM) chirp pulses are employed for the transmission and reception of reflection pulses both to and from the object being detected. The advantages of using LFMs include their higher signal-to-noise ratio and lower hardware complexity, when compared to short impulses [9]. The pulses received at the radar are then passed onto a processing algorithm, as proposed in this paper, for detection confirmation. The processing procedure is divided into two parts, namely pre-processing and post-processing. Pre-processing involves pulse extraction from the received signals, whilst post-processing involves the necessary analysis required to generate an image of the scanning area.

In a bid to prove the validity of the proposed model, a theoretical analysis is given, followed by a series of field experiments, using a prototype. The results indicate that the proposed system can detect and localize objects as small as 2 cm high and 1 cm diameter, located several metres away. With the use of lower frequencies, the system may also used for other applications, such as mine detection and through the wall detection, as experimented in [10], where a linear movement ground-based SAR was used to detect 15 cm bolts behind a 10 cm wall a few meters apart. Also some medical applications are conceivable, a similar system is used in [11] for breast tumour localization. In addition, system resolution analysis confirms that the proposed system can distinguish multiple objects in close proximity to each other. A bistatic version of the proposed system is also under investigation, in this way, the RCS prediction method as in [12], and the transfer algorithm proposed in [13] may be used.

Section 2 discusses the cross-range imaging of Circular-SAR in detail, whilst Section 3 discusses the experimental aspects of the system. The Detection and Localization Algorithm is proposed in Section 4, whilst Section 5 discusses the resolution of the system. The paper is concluded in Section 6.

2. LFM C-SAR SYSTEM

Synthetic Aperture Radar (SAR) is a well-known technique for taking high resolution pictures [14], and has been employed in a variety of applications. Air and space-borne SAR has attracted interest for many years [15]. Several ground-based SARs have been developed mainly for extracting geophysical and interferometric information [16]. An especial model of Circular-SAR is introduced in this paper. The range imaging mechanism, employed in the proposed Circular-SAR, is the usual technique employed in linear SAR, as mentioned in literatures

such as [5, 6];, so more attention will be paid to its cross-range imaging.

From an information theory point of view [5], it is possible to retrieve one-dimensional object information (i.e., in the cross-range domain) from a one dimensional measurement (i.e., the synthetic aperture domain). This implies that cross-range imaging is not dependent on the transmitted signal's characteristics. Hence, for mathematical convenience, a single frequency Continuous Wave (CW) signal can be used. However, 2D SAR imaging is afforded by using a wideband signal. Here, two different time domain scenarios are considered, namely the slow-time domain 'τ', and the fast-time domain 't'. In addition, in the 2D imaging, a stop-and-go method was used, which implies that the antennas appear to be stationary, whilst the pulse is being sent and received, before the antennas move to the next position. This assumption is fair and common in SAR, due to the huge differences between slow-time and fast-time.

2.1. Circular-SAR Cross-range Imaging through Matched Filtering

In circular-SAR, range and cross-range directions correspond to the cylindrical coordinates, contrary to linear SAR, which can be presented in Cartesian coordinates. Generally, a finite object can be considered as a set of different isotropic points, with different RCS [5]. For generating a cross-range image of objects at identical distances, the points must have an equal range from the sensors. As shown in Figure 1, the object

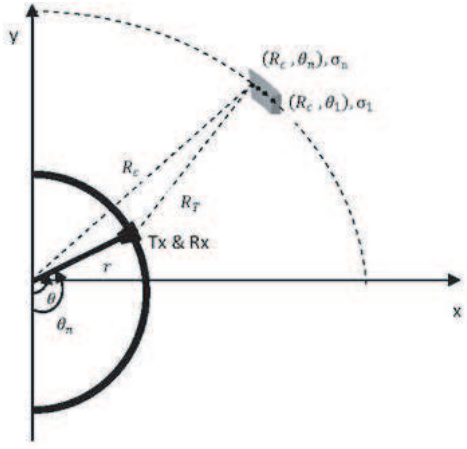

Figure 1. System geometry for cross-range imaging.

is regarded as a number of points with the coordinate (R_c, θ_n), where R_c is their common range and $\theta_1\,\theta_2\,\ldots\theta_n$ are their different angles. The Radar Cross Section of each point is shown as $\sigma_1\,\sigma_2\,\ldots\sigma_n$, and hence, the target reflectivity $f_0\,(\theta)$ is given by [5, 17]:

$$f_0(\theta) = \Sigma_n \sigma_n \delta(\theta - \theta_n) \tag{1}$$

where, $\delta\,(\theta)$ is the Dirac delta function, representing an ideal object return. The aim of the cross-range imaging procedure is to produce this target reflectivity, in order to show each point-object.

For a thorough analysis of the received signal, it will be assumed that the transmitter is sending a single frequency signal, such that:

$$p(t) = \exp(j\omega t) \tag{2}$$

The effect of all the points can be added together, in order to see the actual signature of the whole object. Theoretically, a continuous summation should be used, which is an integral. However, using a discrete summation is valid [5]. The recorded received signal, as θ varies, can be expressed as:

$$s(t, \theta) = \Sigma_n \sigma_n p(t - t_d) \tag{3}$$

where, 't_d' is the time-delay that the wave experiences, to reach the receiver. The distance the signal travels is:

$$R_T = \sqrt{\left[r^2 + R^2 - 2rR_c\cos(\theta - \theta_n)\right]} \tag{4}$$

hence

$$\begin{aligned} s(t,\theta) &= \sum_n \sigma_n p\left[t - \frac{2 \times \sqrt{[r^2 + R^2 - 2rR_c\cos(\theta - \theta_n)]}}{c}\right] \\ &= \exp(j\omega t)\Sigma_n\sigma_n \exp\left[-j2k\sqrt{[r^2 + R^2 - 2rR_c\cos(\theta - \theta_n)]}\right] \end{aligned} \tag{5}$$

where, $k = \omega/c$ is the wave number. The point $\theta = \theta_n$ is the point at which the transmitting antenna directly faces to the point object. This point is called the Closest Point of Approach (CPA) for the nth object.

After baseband conversion in fast-time, performed in a nonlinear device, the received signal will be:

$$s(\omega, \theta) = s(t, \theta)\exp(-j\omega t) \tag{6}$$

It can be seen that this function is not dependent on fast-time 't', and it only depends on the transmitted frequency ω. Hence, it is indicated as $s\,(\omega,\, \theta)$.

Considering the baseband signal for a unit reflector at the centre of a broadside object area (i.e., when $\theta_n = \theta_c$), the reference signal is given by:

$$s_0(\omega, \theta) = \exp\left[-jk\sqrt{[r^2 + R^2 - 2rR_c\cos(\theta - \theta_n)]}\right] \tag{7}$$

Hence, each arbitrary received signal, $s\,(\omega,\, \theta)$ can be expressed as:

$$s(\omega, \theta) = f_0(\theta + \theta_c) * s_0(\omega, \theta) \tag{8}$$

where, $f_0\,(\theta + \theta_c)$ represents the object, thus:

$$s(\omega, \theta) = [\Sigma_n \sigma_n \delta(\theta - (\theta_n - \theta_c))] * s_0(\omega, \theta) \tag{9}$$

By denoting k_θ as the spatial frequency of the synthetic aperture θ, the received signal in a slow-time Doppler frequency domain, becomes:

$$S(\omega, k_\theta) = F_0(\theta + \theta_c) S_0(\omega, k_\theta) \tag{10}$$

where, F_0, S_0 are the f_0, s_0 in the Doppler frequency domain. By computing the inverse of the reference signal S_0, we can attain $F_0(\theta + \theta_c)$ as follows:

$$S(\omega, k_\theta) \cdot S_0^{-1}(\omega, k_\theta) = F_0(\theta + \theta_c) S_0(\omega, k_\theta) \cdot S_0^{-1}(\omega, k_\theta) \tag{11}$$

Hence,

$$F_0(\theta + \theta_c) = S(\omega, K_\theta) \cdot S_0^{-1}(\omega, k_\theta) \tag{12}$$

And its slow-time domain counterpart is expressed as:

$$f_0(\theta + \theta_c) = s(\omega, K_\theta) \cdot s_0^{-1}(\omega, k_\theta) \tag{13}$$

where, (11) and (12) can apply to the unknown received signal as the matched filtering, in order to get the ideal target reflectivity, which represents the object position in slow-time.

3. LFM CIRCULAR-SAR EXPERIMENTATION

The proposed LFM Circular-SAR system consists of a transmitter and a receiver antenna, installed on an arm, which rotates slowly around a tower, to scan a 180-degree swath. A train of pulses is sent continuously, and their reflections are recorded for further processing. Figure 2(a) shows the layout of the proposed system for ground object detection. The horn antennas, the arm, and the computer-controlled stepper motor, are shown in Figure 2(b). The system is launched over an asphalt-covered clear field, which is similar to an airport runway. The height of the tower and the antennas' tilting angles are adjusted iteratively until the position with the best signal strength is attained.

Several typical FOD objects were tested, namely metallic cylinders of 1 cm diameter and $1.5 \sim 2.5$ cm heights, a SMA-BNC connector, and several coins joined together to form a cylindrical shape. The dimensions of these objects are illustrated in Figure 3.

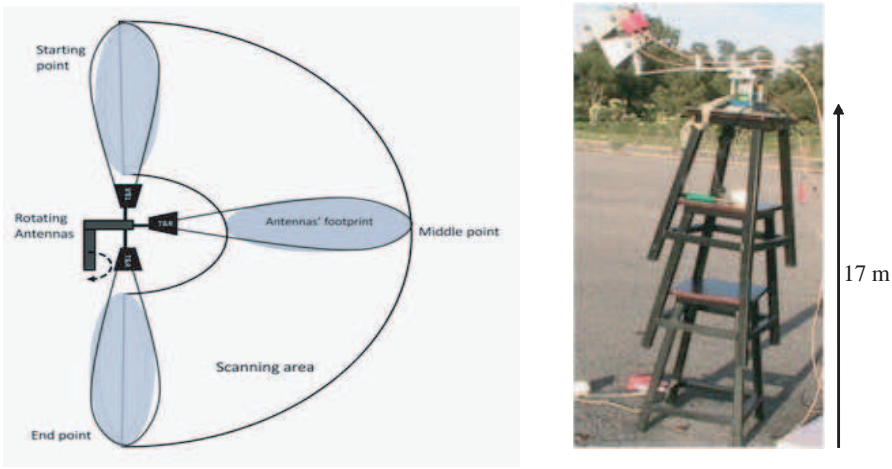

(a) (b)

Figure 2. The proposed system, (a) schematic, (b) the transmitter & receiver parts.

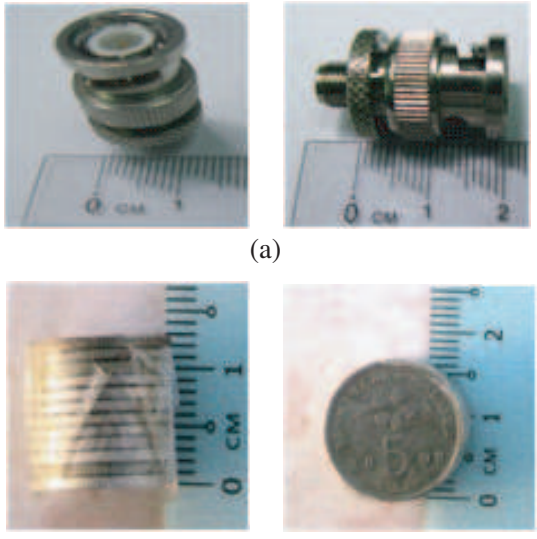

Figure 3. The sizes and shapes of the objects, (a) SMA-BNC connectors, (b) several coins taped together.

3.1. Signal Properties

The signal used for the proposed radar system is a Linear Frequency Modulated (LFM) pulse, which comes with several advantages. Firstly, it helps in achieving a high detection capability of a long pulse, while retaining the range resolution of a narrow pulse. Secondly, LFM pulses significantly reduce hardware complexity e.g., sampling frequency [9]. A LFM pulse can be generated in different methods like FPGA and DDS [18] and is formulated as follows [5, 15]:

$$p_T(t) = a(t) \exp\left(j\beta t + j\alpha t^2\right) \tag{14}$$

where, $a\,(t)$ is a rect function, where $a(t) = 1$ for $0 \leq t \leq T_p$, and $a(t) = 0$ otherwise. T_p is the pulse duration. The instantaneous frequency of the chirp, which is a derivative of its phase function with respect to time, is given by:

$$IF = \frac{d}{dt}\left(j\beta t + j\alpha t^2\right) = \beta + 2\alpha t, \quad 0 \leq t \leq T_p \tag{15}$$

where, α is the chirp rate. It can be noticed that the chirp frequency sweeps from β to $\beta + 2\alpha T_p$ in the pulse duration, hence the carrier frequency can be calculated as:

$$F_c = \beta + \alpha T_p, \tag{16}$$

And its baseband bandwidth is:

$$BW = \alpha T_p. \tag{17}$$

It can be seen that the chirp bandwidth depends on the chirp rate and pulse duration. Figure 4 shows an apt illustration of a practical transmitted signal during the experiment.

Figure 4(b) shows the LFM pulse, sweeping from 6 GHz to 7.5 GHz in 10 ms, which is repeated every 30 ms. However, Figure 4(a) shows

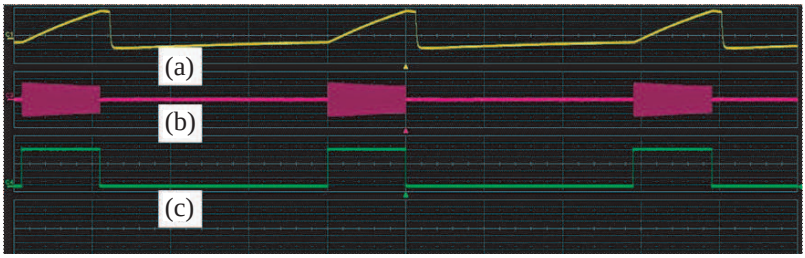

Figure 4. Experimental transmitted signal observed in the oscilloscope.

Table 1. System characteristics in circular-SAR.

Bandwidth	1.5 GHz
Carrier frequency	6.75 GHz
Chirp duration	10 ms
Chirp rate, α	1.5×10^{11} Hz/s
Pulse Repetition Interval	40 ms
Sampling frequency	50 kHz
Scanning time	52.180 s

the instantaneous frequency, which increases linearly during the pulse duration as expected from the Equation (15). Figure 4(c) is the envelop pulse used to trigger the sweep generator. This pulse is also used for synchronization purposes, which will be discussed in detail, later in this paper. The characteristics of the system and the transmitted signal are shown in Table 1.

3.2. Pulse Compression

When the object is being illuminated by the transmitted signals from the radar, the reflected signals received at the receiver exhibit an identical shape as the original signal;, and the only differences are in their amplitudes and time delays. The amplitude of the chirp pulse also depends on the position of the antenna, which rotates slowly. Without loss of generality, the amplitude can be considered as a function of slow time 'τ'. Therefore, the transmitted LFM pulse can be computed using:

$$p_T(t) = \alpha(t, \tau) \exp\left(j\beta t + j\alpha t^2\right) \tag{18}$$

Based on the stop-and-go assumption, the pulse will illuminate the object and reflect back to the receiver within a time limit, where the instantaneous change in position is finitely very small. Hence, the received pulse is given by:

$$p_R(t) = a(t - t_d, \tau)\sigma \exp\left(j\beta(t - t_d) + j\alpha(t - t_d)^2\right) \tag{19}$$

where, 'σ' is the signal amplitude, which represents the reflectivity and total path lost. And 't_d' is the time delay, which can be expressed as $t_d = 2R/c$, where R, C are the slant range and speed of light, respectively.

If the homodyne receive circuit is used, by neglecting the effect of t_d in the envelope of the pulse, the recorded signal will be:

$$\begin{aligned} P_{rec}(t) &= p_T(t) * p_R(t) \\ &= \frac{\sigma a(t,\tau)^2}{2} \cos\left[2\pi\left(\beta t+\alpha t^2\right)\right] \cos\left[2\pi\left(\beta(t-t_d)+\alpha(t-t_d)^2\right)\right] \\ &= \frac{\sigma a(t,\tau)^2}{2}\left\{ \cos\left[2\pi\left(\beta t+\alpha t^2\right)+2\pi\left(\beta(t-t_d)+2\pi\alpha(t-t_d)^2\right)\right]\right. \\ &\quad \left. + \cos\left[2\pi\left(\beta t+\alpha t^2\right)-2\pi\left(\beta(t-t_d)-2\pi\alpha(t-t_d)^2\right)\right]\right\} \quad (20) \end{aligned}$$

Here, the first sinusoidal signal is a high frequency, because α, β are normally large values in comparison to t_d. The second low frequency term and its harmonies can easily be separated by using a low pass filter, and this will reduce the equation to:

$$\begin{aligned} p_{rec}(t) &= \frac{\sigma a(t,\tau)^2}{2} \cos\left[2\pi\left(\beta t+\alpha t^2\right)-2\pi\left(\beta(t-t_d)-2\pi\alpha(t-t_d)^2\right)\right] \\ &= \frac{\sigma a(t,\tau)^2}{2} \cos\left[2\pi\left(2\alpha t_d t+\beta t_d-\alpha t_d^2\right)\right] \quad (21) \end{aligned}$$

As it shown, the recorded signal is a frequency-modulated signal with $2\alpha t_d$ frequency and $(\beta t_d - \alpha t_d^2)$ time delay. As such, by measuring its frequency and having α, the magnitude of t_d can be evaluated.

A schematic circuitry diagram of the transmitter and the receiver is shown in Figure 5. Here, a signal generator is used to generate the

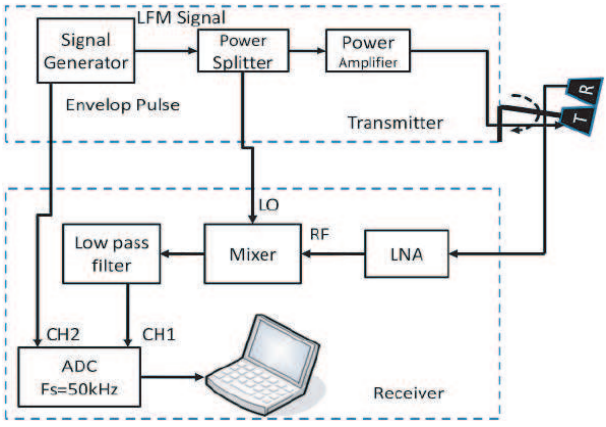

Figure 5. Schematic view of the transmitter and the receiver circuit.

LFM, as well as the envelop pulse. In turn, the envelop pulse is used to extract the pulses in a synchronous manner. The signal generator RF output is split into two parts: one is used for transmitting (after amplification), whilst the other is used as a reference local oscillator in the receiver. The received signal in each receiver is amplified and down-converted using a mixer, prior to filtering of the double frequency, using a low pass filter [19].

The mixer, which is a nonlinear device, multiplies the received signal with the reference signal. The output of the mixer is comprised of both low and high frequency parts as shown in Equation (20). By using a Low Pass Filter (LPF), the low frequency part can be recorded by a low-cost Analogue to Digital Converter (ADC). By concurrently sending the LFM pulse train during the scanning period, and recording the received signal, a long-period pulse train signal is acquired. Considering the scanning time and pulse width, the scanning area is divided into $52.180/0.04 \cong 1,304$ arcs. In this way, 1,304 pulses are recorded.

The envelop pulse in channel 2 is synchronized with the pulse train and can be used to extract the pulses, thereby ensuring coherent signal processing. While receiving this train of pulses, the antennas keep rotating, and hence, each pulse carries information about the scanning area, in that instant of time. The first pulse in the train corresponds to *ST=1*, which is the starting position, the 650th pulse depicts *ST=650,* which is the point where the antennas cross the middle line, and the last pulse indicates the stopping position.

3.3. Signal Pre-processing

A pre-processing algorithm for the proposed system was introduced, as shown in Figure 6. Firstly, the start of each pulse is detected by finding the positive edge of the envelop pulse. Then, a certain length of the signal is recorded, based on the pulse duration and sampling frequency. A Hilbert-Huang Transform (HHT) [20, 21] is applied to the pulse, to filter the DC value. Proper Fast Fourier Transform (FFT) is then applied to the resultant pulse, in order to convert it into the frequency domain.

Each point in the frequency domain corresponds to a slant range, and hence, its amplitude value represents the reflectivity of the object, within that specific range. The relationship between range and frequency beat, is given by [5]:

$$f_{\text{beat}} = 2\alpha t_d = 4\alpha R/c \tag{22}$$

The total time delay of the signal consists of a delay in free space and a circuit delay, including delay in cables, connectors, components, etc..

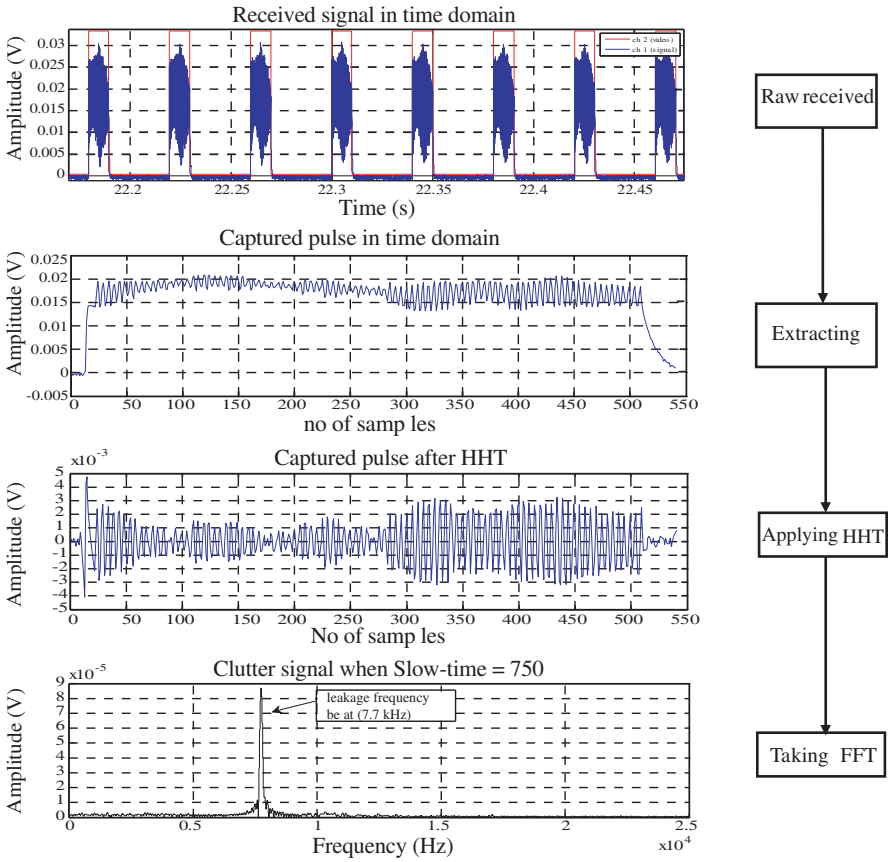

Figure 6. Pre-processing algorithm.

Thus, Equation (22) can be rewritten as:

$$f_{\text{beat}} = f_{cd} + 2\alpha t_d = f_{cd} + 4\alpha R/c \tag{23}$$

where, 'f_{cd}' is the frequency, due to circuit delay. As 'f_{cd}' is difficult to measure, a more calibrated formula is used as follows:

$$f_{\text{beat}} = f_1 + \frac{2\alpha}{c}(2R - 1) \tag{24}$$

where, f_1 is frequency beat caused by a reference point at 0.5 m slant range from the antennas.

The slant range can be converted to ground range R_g, by:

$$R_g = r + \sqrt{R^2 - h^2} \tag{25}$$

where, r is the antenna arm-length and h is the tower height.

As shown in Figure 6, a clear frequency beat exists at 7.7 kHz. This is due to the direct leakage between the transmitter and receiver antennas, which can be verified by changing the Tx-Rx distance. This distance is only a few centimetres, as shown in Figure 2(b), while the minimum scanning range is more than 2 metres. Therefore, the leakage frequency does not interfere with the actual signals.

Figure 7 shows the clutter signal in terms of range, which is afforded by converting the frequencies shown in Figure 6 into ground ranges using Equations (24) and (25). The lower range is selected based on the application's requirements, whilst the upper range is due to the inherent limitations of the digitizing equipment.

Based on the number of points used in the FFT, the output of the proposed pre-processing algorithm provides a matrix where the number of rows is as the number of pulses in the signal (i.e., 1,304 in this case) and the number of columns is NFFT/2 (i.e., the number of FFT points divided by 2).

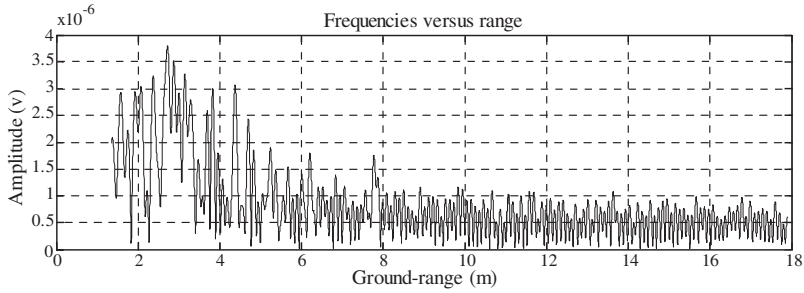

Figure 7. Clutter signal in different ranges.

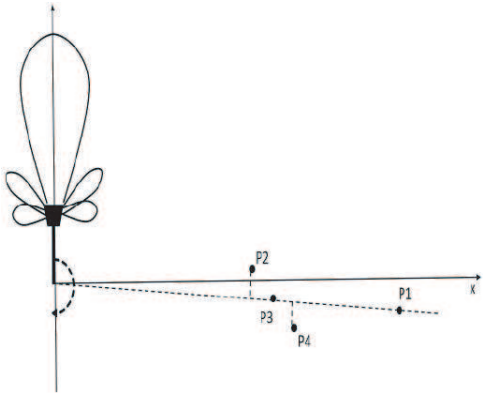

Position	Range (m)	Angle (degree)
P1	10	-18^o
P2	6.6	-10^o
P3	7	-18^o
P4	7.40	-22^o

Figure 8. Different object positions.

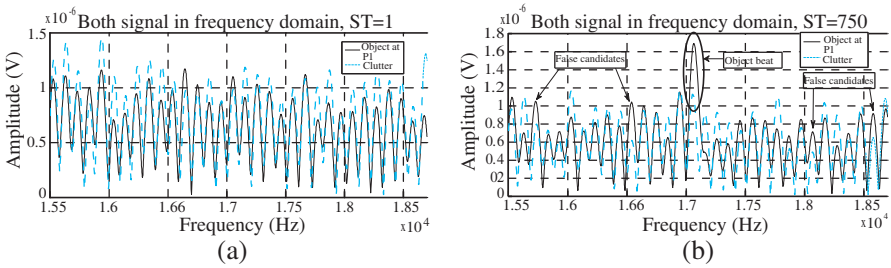

Figure 9. Expanded views of both signals for different slow-times. (a) Slow-time = 1 (i.e., object out of the scope). (b) Slow-time = 750 (i.e., object in the scope).

To analyse the system's ability in detecting and localizing small objects, several positions were considered at various ranges and angles, as shown in Figure 8. The system is first run over a ground-only scene, in order to collect a clutter signal. Next, the object is placed at the position and scanned with the radar system. By applying the pre-processing algorithm, a data matrix, which is of the same size as the clutter matrix, is achieved. Using the LFM range analysis, the object produces a frequency beat at 17.1 kHz.

Figure 9 shows the clutter signal, as well as the signal when the object is putted at $P1$. In Figure 9(a), where $ST{=}1$ (i.e., the starting point of the rotation), the object is not within the scope of the antennas. Therefore, both the object and clutter signals are almost identical. However, when the antennas face the target, the presence of the object creates a small beat at 17.1 kHz, as shown in Figure 9(b).

As can be seen in Figure 9(b), several other peaks may also appear in addition to the object beat. These may be due to thermal noise, quantizing noise, multiplicative noise (i.e., a small instability of the radar), or even a moving insect or leaf within the area. By discarding their source as noise signals, they are identified as false candidates in future processing. In order to distinguish the real object from the false candidates, its effect is traced in all slow-time signals. In this way, the real object follows the antenna's pattern, while the false candidates do not. This is the main idea for developing a post-processing algorithm.

3.4. Data Matrices

The resultant matrix, upon applying the pre-processing algorithm on the clutter signal, is a $1,304 \times \mathrm{NFFT}/2$ matrix, whose rows represent the different slow-time positions of the antennas. Meanwhile, each column represents a frequency of the slant-range of the object, within the vicinity of the antennas.

Another matrix, with the same dimensions as the first, could be constructed from the object signal, i.e., when the object is at $P1$ (as shown in Figure 8). Figure 10 shows the raw and column views of both matrices, where the object signal is indicated in bold, whilst the clutter is indicated in a lighter colour. Each row of the matrices shows all frequencies in the slow-time, where Figure 10(a) shows a zoomed-in-view between 15 kHz and 19 kHz. Different slow-times are shown. The object's signature appears in the region, where the object falls within the beam of the antennas (e.g., $ST = 680 \sim 900$), as indicated by the space enclosed in the dashed rectangle in Figure 10(a).

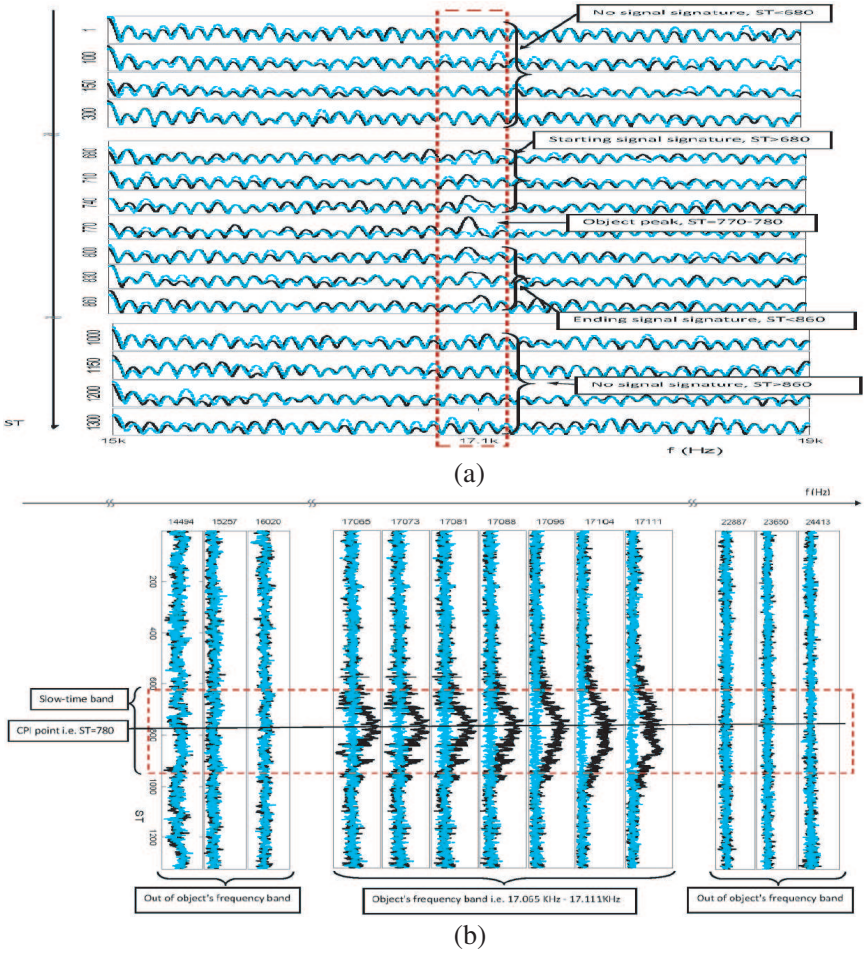

Figure 10. Data matrix samples for object at $P1$. (a) Row view. (b) Column view.

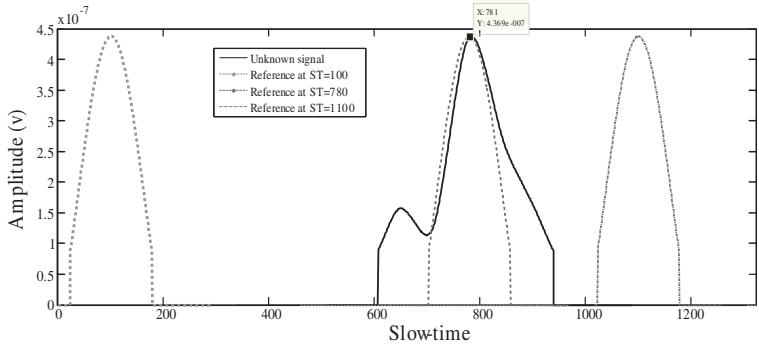

Figure 11. Slow-time match filtering.

On the other hand, Figure 10(b) shows each frequency in all slow-times. From the range measuring Equations (24) and (25), the expected frequency beat, which was created by the object at $P1$ position, is 17.1 kHz. This coincides with Figure 10(b), where the object signature appears only in the space enclosed by the dashed rectangle. Since the object under test is relatively large compared to the range resolution of the system, the object's detection is featured in a band of adjacent frequencies, as shown in Figure 10(b).

In order to find the position of the object in slow-time, the object's signature (shown in Figure 10(b)) is compared with the antennas' pattern. In this way, several shifted copies of the antennas' main lobe, in the different slow-time positions, are used as reference signals for the cross-range imaging technique, in circular-SAR. The reference signals are then normalized by the object signal. At this stage, the clutter signal is removed from the object signal using adaptive filtering or the standard subtraction function, followed by smoothing using the wavelet de-noise functions, the noise cancellation method proposed in [22] may also applicable. After smoothing, the resultant signal is then compared with the reference signal, where the two signals match, the slow-time will be selected as the found position. The unknown object signature and references at the different slow-times are shown in Figure 11. By comparing each reference signal with that of the object, the reference signal that has the highest resemblance with the object signal is chosen (i.e., at *ST=780* in the case of Figure 11 because the object's peak signature is located at *ST=780,* based on its location dimensions).

3.5. Detection and Localization Algorithm

The implementation of the object detection and localization algorithm constitutes the post-processing part of the proposed system. It could

be recalled that the output from the pre-processing stage consisted of two data matrices of the same size, namely clutter and object. During the post-processing stage, there were two options: either the clutter can be removed from the object signal, showing only the object, or the original object signals can be analysed without removing the clutter, in order to have a complete view of the area.

Specifically, the scanned area ranges are converted into a frequency domain. Each frequency slice is associated with a slow-time signature, as shown in Figure 10(b). This signature is compared with the shifted reference signal after de-noising and normalization, and the reference is found to be identical to the object signature, constituting a peak; otherwise a flat (zero) output is generated. This process is repeated for all frequencies defined in the frequency domain, thereby generating a new matrix with as many rows as there are slow-times (i.e., 1,304 in this case) and as many columns as defined by the area width. This matrix is the image of the scanned area, as illustrated in Figure 12 when the object is positioned at $P1$.

As Figure 12 shows, each object is indicated as a point in general view (i.e., when zoomed-out). However, by zooming in, each point consists of a cluster of adjacent points in close proximity. Figure 13 shows the zoomed-in image around $P1$. This confirms the idea that despite the minute nature of the object, it can in fact be considered as a number of separate points, where each of them can generate a unique frequency [5]. In this way, the object as a whole can be represented as a band of frequencies. In Figure 13 for example, the distance range covered by the object effect (which is the maxima and minima of the points in range), is 9.9975 m–10.0068 m. The total width of which is approximately 1 cm, which is a fine resolution for this application.

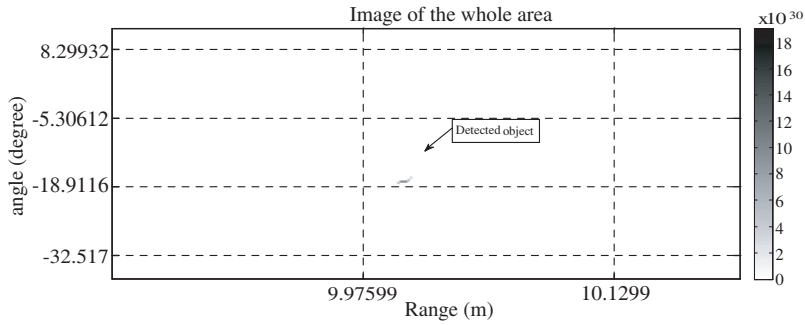

Figure 12. Image of the scanned area when the object is at $P1$.

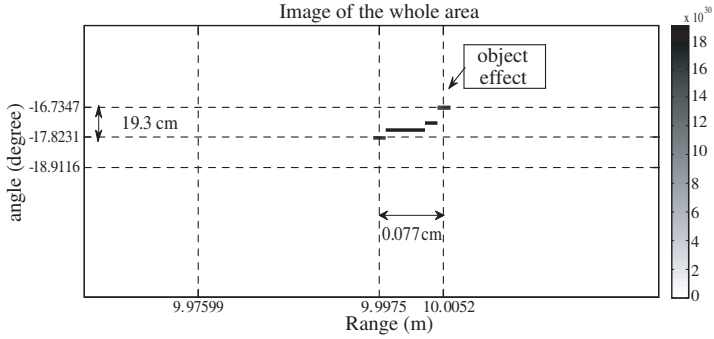

Figure 13. Image of the scanned area, zoomed in around $P1$.

4. MULTIPLE OBJECTS AND RESOLUTIONS

Generally, resolution is evaluated in two dimensions, namely range and cross-range. The latter is sometimes known as azimuth, or along-track, in some SAR systems.

4.1. Range Resolution

Range resolution generally depends on the bandwidth of the transmitted signal. Hence, it remains the same for both synthetic and real aperture radar (SAR or RAR) applications. As indicated in Equation (21), the frequency of the recorded pulse, after applying pulse compression, is $2\alpha t_d$. Supposing δ_R as the difference between two separate point-objects in range (i.e., range resolution), the difference in their frequencies is given by:

$$\delta_f = 2\frac{\alpha}{c}\delta_R \tag{26}$$

So:

$$\delta_R = \frac{\alpha}{c}\delta_f \tag{27}$$

The minimum measurable δ_f depends on the system's ambiguity function. Normally, range resolution is given by [23–25]:

$$\delta_R = \frac{c}{2B} \tag{28}$$

By substituting the indicated values of parameters B and c in Table 1, the range resolution (δ_R) is 10 cm, which is the usual theoretical value. This theoretical value is further supported by the experimental results, and thus, even two objects that are as close as 10 cm distance in range, can be seen clearly using the proposed circular-SAR prototype.

4.2. Cross-range Resolution

The main aim of SAR systems is to improve cross-range resolution, which can be attained using various methods, depending on the underlying assumptions [26]. For example, in [26], it is assumed that the illumination time is sufficiently short such that the matched filter can be generated by expanding the second order of the phase of the received signal. This requires the change in angle of view ($\Delta\varphi$) to be much smaller than one (i.e., $\Delta\varphi \ll 1$). However, in the proposed SAR, this assumption does not hold true, and hence, cannot be employed.

The method that suits the proposed system, is possibly presented in [26], where the variation of angle view during illumination time, is considered to evaluate the cross-range resolution. In the proposed system, the variation of angle view is shown in Figure 14, in which:

$$\Delta\varphi = \varphi_1 + \varphi_2 \tag{29}$$

where, φ_1 and φ_2 are the angles formed when the antenna pattern covers the object on both entering the object zone, and leaving it, respectively.

The Doppler frequency of the received signal, during the variation time as calculated in [27], is:

$$f_{D1} = r\Omega/\lambda \sin(\pi - \theta_{3\text{dB}} - \varphi_1) = -r\Omega/\lambda \sin(\theta_{3\text{dB}} + \varphi_1) \tag{30}$$

$$f_{D2} = -r\Omega/\lambda \sin(\pi - \theta_{3\text{dB}} - \varphi_2) = r\Omega/\lambda \sin(\theta_{3\text{dB}} + \varphi_2) \tag{31}$$

where, r, Ω, λ and are $\theta_{3\text{dB}}$ the arm length, rotation angular velocity, carrier wavelength, and antenna 3 dB beam angle, respectively.

Although the Doppler signal is not linearly frequency modulated, its equivalent bandwidth remains close to:

$$B_D = 2\sqrt{\pi}\left(\frac{\int_{-\infty}^{+\infty} f^2|s(f)|^2 df}{\int_{-\infty}^{+\infty} |s(f)|^2 df}\right) \approx f_{D2} - f_{D1} \tag{32}$$

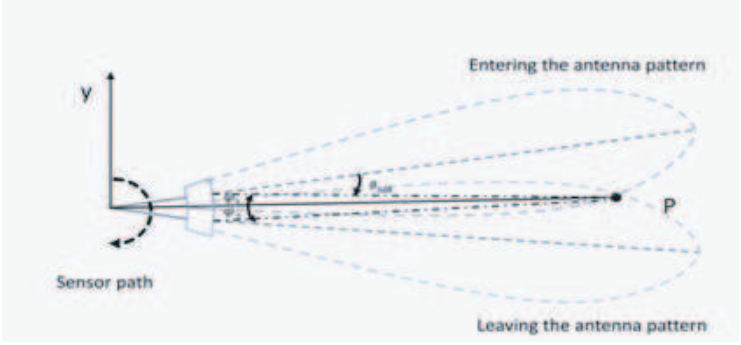

Figure 14. Variation of angle view.

The width of correlation peak at 3 dB can be evaluated as [26, 28]:

$$\Delta\tau \approx \sqrt{\frac{2}{\pi}}\frac{1}{B_D} \approx \frac{\sqrt{2}}{\sqrt{\pi}(f_{D2} - f_{D1})} \tag{33}$$

Thus, the cross-range resolution is given by:

$$\delta_{CR} = \upsilon\Delta\tau = r\Omega\Delta\tau = \frac{k\lambda}{\sin(\theta_{3\text{dB}} + \varphi_2) + \sin(\theta_{3\text{dB}} + \varphi_1)} \tag{34}$$

where, $k = 1/\sqrt{2\pi}$.

In Equation (33), $\theta_{3\text{dB}}$ is fixed and depends on the antennas' specifications. However, angle views vary for different ranges. However, the cross-range resolution in worst case will be around few centimetres. During the experiments, the cross-range resolution was limited by the number of slow-times. The 180° spotlight area is scanned during each rotation. LFM pulses are regenerated each 40 msec (as shown in Table 1). In this way, the total slow-time is the ratio of the scanning time to the pulse duration (i.e., 1,304 slow-times during the experiment). The angle resolution (δ_{ang}) is defined as the ratio of the scanning angle to the slow-time, mathematically,

$$\delta_{ang} = \pi/ST$$

The cross-range resolution depends on the object's range [8] and can be calculated as:

$$\delta_{CR} = R\sin(\delta_{ang}) \cong R\delta_{ang} = R\pi/ST$$

For example, δ_{CR} at a 10 m range in the experiment, where *ST=1,304*, will be:

$$\delta_{CR10} = 10 \times \frac{\pi}{1304} \cong 24\,\text{cm}$$

Meanwhile, at a 5 m range, it will be:

$$\delta_{CR5} = 5 \times \frac{\pi}{1304} \cong 12\,\text{cm}$$

By increasing the scanning time (i.e., the illumination time), the cross-range resolution can be reduced.

In order to evaluate the system's resolution during the experiment, three objects were arranged close to each other, at points *P6, P7, and P8* (as shown in Figure 8, where $d = 40$ cm grid). Figure 15 shows the actual objects.

In Figure 16, the scanning results of these objects are illustrated, where the objects are detected and displayed as a cluster of points.

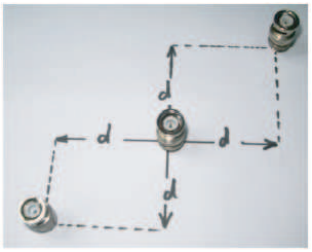

Figure 15. Multiple objects.

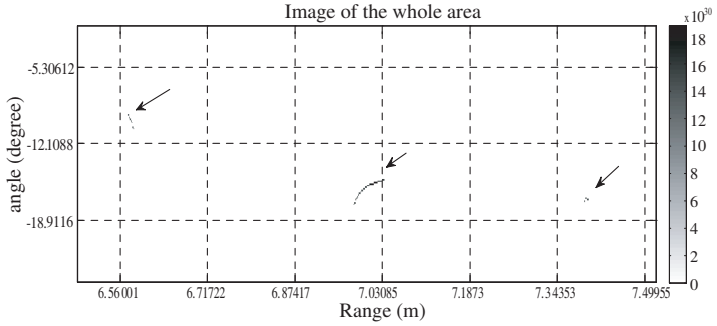

Figure 16. Image of the scanned area, 3 objects at $P2$, $P3$, and $P4$.

5. CONCLUSION

In this paper, a circular-SAR system for detecting an small on-the-ground object has been proposed. One possible application of such a system is runway FOD detection. The proposed system was first analysed mathematically, and based on it, a prototype was developed for further experimentation. Here, transmitter and receiver antennas were installed on a projected arm that rotates slowly about a pivot, with the aid of a pc-controlled stepper motor. A Linear Frequency Modulated chirp signal, with a 1.5 GHz bandwidth, was used. Several experiments were performed to detect a small 1×2 cm cylindrical object, at various distances. A pre-processing algorithm was then introduced to extract the pulses, which were then passed through a post-processing algorithm, to generate a resultant image. From the results, it was found that the proposed SAR system is capable of detecting and localizing small on-ground-objects, located several metres from the antenna. Moreover, multiple objects located near to each other can be identified and localized separately. As such, it is concluded that the proposed SAR system could be a suitable alternative for use in FOD detection applications after some

modifications. The direction for future work includes developing a circular-SAR processing algorithm, using tools that will be attained through simulation of the system. In addition, increasing the coverage of the proposed system and the suitability of the proposed system for behind-the-wall and under-the-ground object detection will also be explored.

REFERENCES

1. Procaccio, F., *Effectiveness of Fod Control Measures*, Embry-Riddle Aeronautical University Worldwide Campus, 2008.
2. O'Donnell, M. J., *Airport Foreign Object Debris/Damage (Fod) Detection Equipment*, Advisory Circular of U.S. Department of Transportation, Federal Aviation Administration, 2009.
3. Patrick, D. L. B. and P. R. D. Qinetiq, "Tarsier® a unique radar for helping to keep debris off airport runways," *The Institution of Engineering and Technology Seminar on the Future of Civil Radar*, 2006.
4. "IEEE Standard Radar Definitions," *IEEE Std*, 686–1997, 1998.
5. Soumekh, M., *Synthetic Aperature Radar Signal Processing with Matlab Algorithms*, 616, John Wiley, New York, 1999.
6. Majumder, U., et al., "Synthetic aperture radar moving target indication processing of along-track monopulse nonlinear gotcha data," *Radar Conference, IEEE*, 2009.
7. Kou, L., et al., "Resolution analysis of circular SAR with partial circular aperture measurements," *8th European Conference on Synthetic Aperture Radar (EUSAR)*, 1–4, 2010.
8. Broquetas, A., et al., "Circular synthetic aperture radar (C-SAR) system for ground-based applications," *Electronics Letters*, Vol. 33, No. 11, 988–989, 1997.
9. Duersch, M. I., "Byu micro-SAR: A very small, low-power, LFM-CW synthetic aperture radar," Master's Thesis, Brigham Young University, Provo, Utah, 2004.
10. Charvat, G. L., et al., "A through-dielectric radar imaging system," *IEEE Transactions on Antennas and Propagation*, Vol. 58, No. 8, 2594–2603, 2010.
11. Lazaro, A., D. Girbau, and R. Villarino, "Wavelet-based breast tumor localization technique using a UWB RADAR," *Progress In Electromagnetics Research*, Vol. 98, 75–95, 2009.

12. Li, X.-F., Y.-J. Xie, and R. Yang, "Bistatic RCS prediction for complex targets using modified current marching technique," *Progress In Electromagnetics Research*, Vol. 93, 13–28, 2009.
13. Sun, J., S. Mao, G. Wang, and W. Hong, "Extended exact transfer function algorithm for bistatic SAR of translational invariant case," *Progress In Electromagnetics Research*, Vol. 99, 89–108, 2009.
14. Chan, Y. K. and V. C. Koo, "An introduction to synthetic aperture radar (SAR)," *Progress In Electromagnetics Research B*, Vol. 2, 27–60, 2008.
15. Chan, Y. K. and S. Y. Lim, "Synthetic aperture radar (SAR) signal generation," *Progress In Electromagnetics Research B*, Vol. 1, 269–290, 2008.
16. Zheng-Shu, Z., W. M. Boerner, and M. Sato, "Development of a ground-based polarimetric broadband SAR system for noninvasive ground-truth validation in vegetation monitoring," *IEEE Transactions on Geoscience and Remote Sensing*, Vol. 42, No. 9, 1803–1810, 2004.
17. Lim, K. S., *Design and Development of Ground Based Radar Systems for Vegetation Studies*, 2009.
18. Chua, M. Y. and V. C. Koo, "FPGA-based chirp generator for high resolution UAV SAR," *Progress In Electromagnetics Research*, Vol. 99, 71–88, 2009.
19. Cherniakov, M., et al., "Automatic ground target classification using forward scattering radar," *Radar, Sonar and Navigation, IEE Proceedings*, Vol. 153, No. 5, 427–437, 2006.
20. Huang, N. E. and S. S. Shen, *Hilbert-Huang Transform and Its Applications*. Vol. 5, World Scientific Publishing Co., Inc., 2005.
21. Chen, W. W., R. C. Chen, and D. Z. Ding, "Application of hilbert-huang transform to MMW doppler radar," *ICMMT Proceedings, International Conference on Microwave and Millimeter Wave Technology*, 21–24, Apr. 2008.
22. Orimoto, H. and A. Ikuta, "Signal processing for noise cancellation in actual electromagnetic environment," *Progress In Electromagnetics Research*, Vol. 99, 307–322, 2009.
23. Goodman, N. A., et al., "Processing of multiple-receiver spaceborne arrays for wide-area SAR," *IEEE Transactions on Geoscience and Remote Sensing*, Vol. 40, No. 4, 841–852, 2002.
24. Pan, J. N., et al., "The performance of LFM signals without components around zero frequency in pulse compression radar," *IET International Communication Conference on Wireless Mobile*

and Computing (CCWMC), 2009.

25. Almorox-Gonzalez, P., et al., "Portable high resolution LFM-CW radar sensor in millimeter-wave band," *International Conference on Sensor Technologies and Applications, Sensor Comm.*, 2007.
26. Lacomme, P., "Air and spaceborne radar systems: An introduction," *Institution of Electrical Engineers*, 2001.
27. Abdullah, R. R., M. Mohammad Poor, A. Ismail, and A. F Abas, "A multistatic circular synthethic aperature radar for small object detection," *IEEE Radar Conference*, 262–266, Kansas City, MO, USA, May 2011.
28. Raney, R. K., "Special SAR techniques and applications," *AGARD Lecture Series 182, Fundamental and Special Problems of Synthetic Aperture*, Neuilly Sur Seine, France, 1992.